IOPscience iopscience.iop.org

Home Search Collections Journals About Contact us My IOPscience

Photoresponse of indium oxide particulate-based thin films fabricated using milled nanorods grown by the self-catalytic vapor–liquid–solid process

This article has been downloaded from IOPscience. Please scroll down to see the full text article.

2012 Semicond. Sci. Technol. 27 045005

(http://iopscience.iop.org/0268-1242/27/4/045005)

View the table of contents for this issue, or go to the journal homepage for more

Download details:
IP Address: 128.113.122.141
The article was downloaded on 20/04/2012 at 21:59

Please note that terms and conditions apply.

Semicond. Sci. Technol. **27** (2012) 045005 (6pp) doi:10.1088/0268-1242/27/4/045005

Photoresponse of indium oxide particulate-based thin films fabricated using milled nanorods grown by the self-catalytic vapor–liquid–solid process

L Qin, P S Dutta and S Sawyer

Electrical, Computer, and Systems Engineering Department, Rensselaer Polytechnic Institute, Troy, NY 12180, USA

E-mail: ssawyer@ecse.rpi.edu

Received 28 November 2011, in final form 30 January 2012
Published 22 February 2012
Online at stacks.iop.org/SST/27/045005

Abstract
Indium oxide (In_2O_3) nanorods were grown on silica substrates by using the self-catalytic vapor–liquid–solid growth process. The photoresponse of the nanorods was compared to that of the thin film, tin-doped indium oxide (ITO). The nanorods demonstrated a wavelength-dependent photoresponse with high responsivity of 1.82 A W^{-1} at 405 nm. In contrast, the conductive ITO thin film did not show a photoresponse to light. Analysis results showed that different surface states of materials as well as doping in ITO contributed to the significant difference in the photoresponse of samples.

(Some figures may appear in colour only in the online journal)

1. Introduction

Indium oxide (In_2O_3) is an amphoteric oxide of indium with bixbyite-type cubic crystals. Its documented bandgap value has recently been revised from the old value 3.7 to 2.9 eV [1, 2]. As an intrinsic *n*-type semiconductor, In_2O_3 has been used as a resistive element in integrated circuits and heterojunction structure with indium phosphide (InP) and gallium arsenide (GaAs) [3]. In combination with tin dioxide (SnO_2), In_2O_3 forms tin-doped indium oxide (ITO), a material used for transparent conductive coatings. The performance of In_2O_3 as a conductive material is well studied. However, its semiconductor properties are not fully understood. Many previous studies mainly focused on the preparations and optical properties (especially light emission) of In_2O_3 nanomaterials due to their beneficial properties, such as quantum confinement effect, high surface area to volume ratio, better absorption than bulk material and high quantum efficiency [4–6]. Currently, electrodeposition by anodic alumina nanoporous structure templates, laser ablation and sol–gel techniques have been used in the synthesis of In_2O_3 nanostructures [1, 4–6]. Research on electrical and optical properties of In_2O_3 nanomaterials is growing [7–12]; however, the photoelectric performance of In_2O_3, to the best of our knowledge, has not been studied yet.

In this paper, In_2O_3 nanorods are synthesized by the self-catalytic vapor–liquid–solid (VLS) growth process. The photoresponse characteristics of In_2O_3 nanorods are measured and compared to those of In_2O_3 thin films with different conductivities. The following analysis shows that surface states in the nanorods cause a change in the Schottky barrier height resulting in a difference in the photoresponse performance.

2. Sample preparation

The In_2O_3 synthesis using a VLS technique was carried out at 1200 °C in continuously flowing oxygen ambient in a tubular furnace. The precursors used for the growth of nanorods were high purity (7N pure) indium films coated around a silica (quartz) tube. The entire growth process occurred within 3–4 h after the furnace reached the growth temperature of 1200 °C. At the end of the growth process, loosened yellow colored In_2O_3 nanorods were grown along the silica tube. The XRD pattern of as-grown nanorods was taken by a Bruker

 © 2012 IOP Publishing Ltd Printed in the UK & the USA

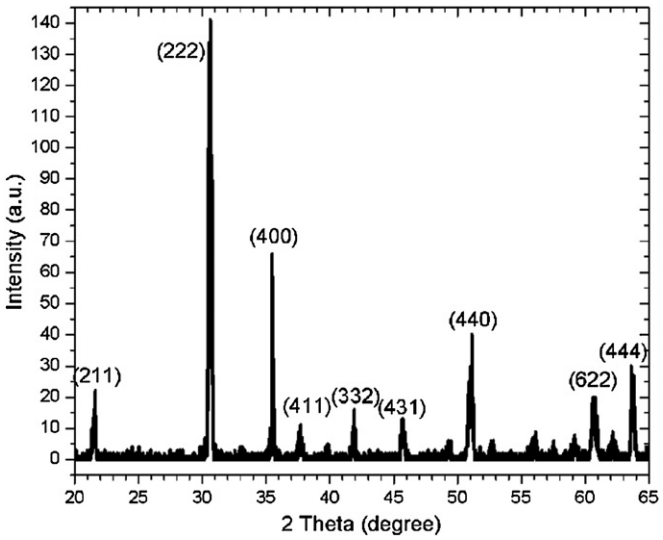

Figure 1. XRD patterns of as-grown In_2O_3 nanorods.

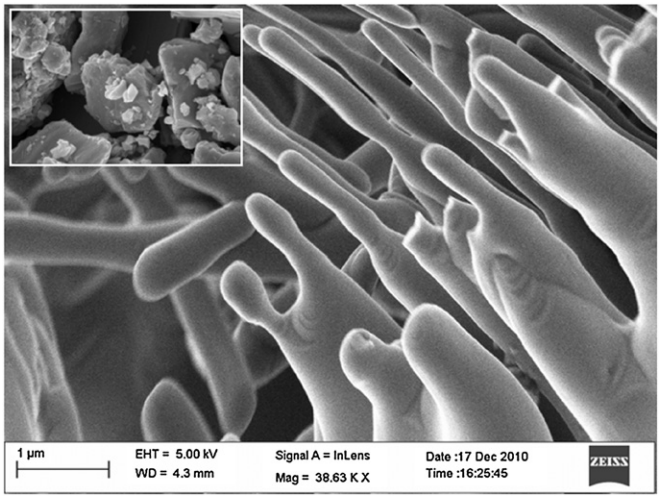

Figure 2. SEM images of In_2O_3 nanorods before and after grinding (inset).

D8 Discover x-ray diffractometer, as shown in figure 1. The crystalline peaks match with the diffraction data of cubic indium oxide (AMCSD 0017267, $a = b = c = 10.12$ Å, $\alpha = \beta = \gamma = 90°$) of high purity. It confirms that the as-grown nanorods are indeed In_2O_3.

The structure and morphology of the In_2O_3 nanorods were then further analyzed by using a Carl Zeiss Ultra 1540 dual beam scanning electron microscope with an accelerating voltage of 5 kV. The images are shown in figure 2, from which we can see that the as-grown nanorods have a wide range distribution in size and length. To prepare shorter nanorods to better deposit onto any substrate for electrical and optical measurements, the synthesized nanorods were ground. After grinding (inset of figure 2), the nanorods were broken into smaller rods significantly, but more surface defects were introduced during the grinding. An attempt to eliminate some of those surface defects was made through annealing in air at 1200 °C for 2–6 h.

Table 1. Parameters of LEDs used in the experiment.

Peak wavelength (nm)	Total optical power within active area (mW)
280 nm	0.3364
340 nm	0.2168
405 nm	0.0358
470 nm	0.0237

The nanorods were then divided into three batches. The first batch (sample A) was dispersed in DI water, coated onto the quartz substrate and then naturally dried in air. A thin film with uniformly distributed In_2O_3 well attached onto the quartz was formed. The second (sample B) and the third (sample C) batches were dispersed in a polyvinyl alcohol (PVA) solution (at 100 °C) with a weight ratio of In_2O_3 to PVA equal to 100:1 and 10:1, respectively. These mixtures were deposited onto quartz substrates and dried in air. Sample B produced a thin film with non-uniform distribution of In_2O_3 though the thin film attached well to the quartz substrate. Sample C produced a uniform plastic thin film with In_2O_3 uniformly distributed, but the film was completely separated from the quartz substrate. A picture of the three samples is shown in figure 3(*a*). The surface morphology and particle distribution of the three samples are shown in the SEM images in figure 3(*b*).

3. Results and discussion

UV–Vis absorption spectra were recorded using a Shimadzu UV–Vis 2550 spectrophotometer in the wavelength range of 200–800 nm. As demonstrated in figure 4, the cut-off wavelengths of In_2O_3 nanorods before and after grinding are the same, about 425 nm (2.9 eV), which is also the same wavelength as that of bulk material. The In_2O_3 nanorods after grinding exhibit an increase in the absorption intensity since smaller size materials are easily attached to and more uniformly distributed onto the quartz substrate.

As shown in the inset of figure 5(*a*), point contact current–voltage (*I–V*) characteristics and the time-resolved photocurrent of samples were measured using a HP4155B semiconductor parameter analyzer under dark and illumination conditions at room temperature in air. The light sources used were light-emitting diodes (LEDs) with parameters listed in table 1. The active areas of samples were 0.007 85 cm^2. Figures 5(*a*)–(*d*) represent the typical *I–V* curves of samples A, B, C and ITO, respectively, with cut-off wavelength at 300 nm which is shown in the inset of figure 5(*d*). Figure 5(*e*) shows a rough spectral responsivity of sample A biased at −20 V based on the information given by figure 5(*a*).

The nonlinear *I–V* responses in figures 5(*a*)–(*c*) show signatures of rectifying effects between the In_2O_3 nanorods and the tungsten needles of the semiconductor parameter analyzer. This rectifying behavior decreases as the conductivity of sample increases (due to the presence of PVA connecting the nanorods, as shown in figures 1(*b*) and (*c*)). The contacts between ITO and tungsten are ohmic as expected. These results indicate that the current conduction mechanism in ITO is different from that in samples A, B and C.

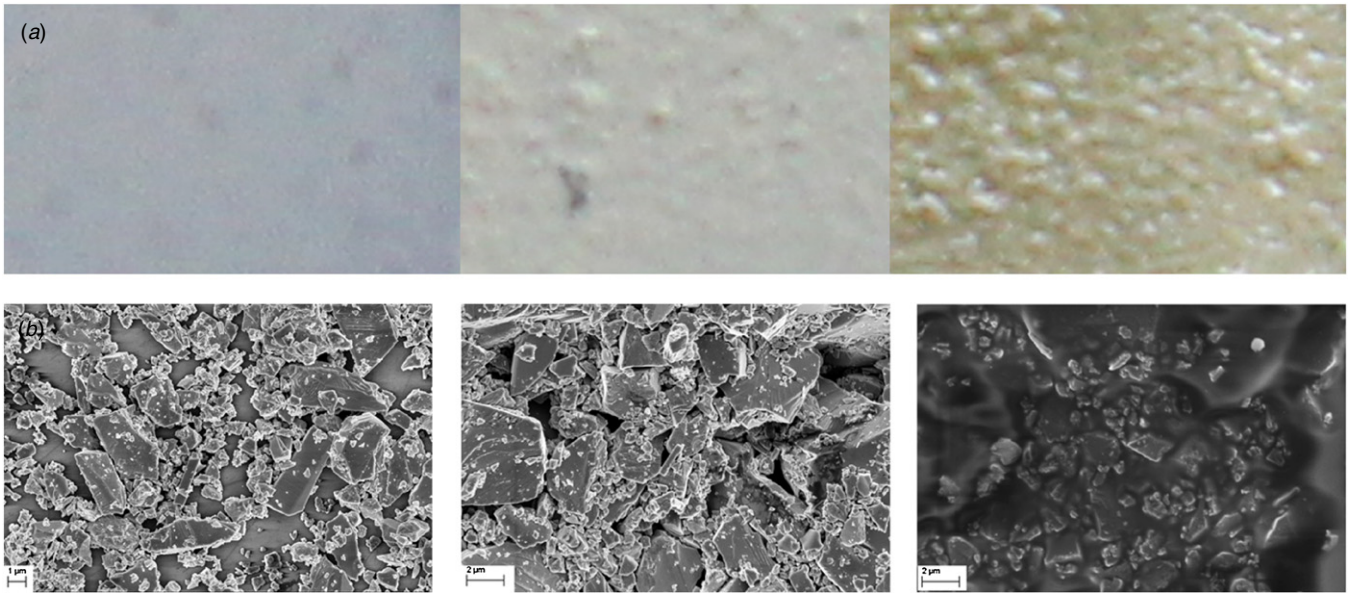

Figure 3. (*a*) Picture and (*b*) SEM images of samples A (In_2O_3), B (In_2O_3 : PVA = 100:1) and C (In_2O_3 : PVA = 10:1) (from left to right).

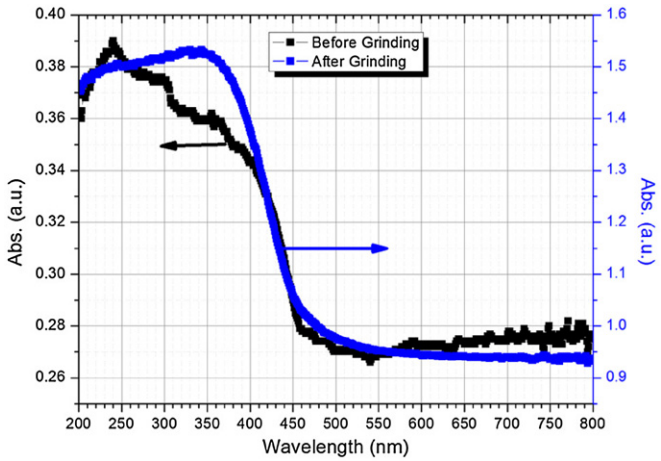

Figure 4. Absorption spectra of In_2O_3 nanorods demonstrate a cut-off wavelength at 425 nm (2.9 eV).

One important parameter to represent the rectified effect of Schottky contact is the barrier height ϕ_B. Based on the thermal emission assumption, the barrier height is given by

$$\phi_B = -\frac{kT}{q} \ln\left(\frac{I_s}{AA^*T^2}\right), \tag{1}$$

where I_s is given by the average dark currents when the applied voltage is 0 [13]. The active area A is 0.007 85 cm^2. The Richardson constant of In_2O_3 is given by

$$A^* = 120\,\alpha \frac{m_e}{m_0}\left(\frac{A}{cm^2\ K^2}\right), \tag{2}$$

where α is an empirical factor on the order of unity, m_e is the effective mass of In_2O_3 and equals $0.3m_0$. Assuming that the empirical factor is 1, for sample A, the barrier height is 0.95 eV which is listed in table 2 with the results of other samples.

For sample A, significant differences between the dark current and photogenerated currents are observed. With 280 nm LED illumination, the ratio of photogenerated current to dark current (on/off ratio) is about 120 at –20 V bias. The ratios of different samples under different illumination situations are listed in table 2. In addition, the wavelength-dependent rough spectral response of sample A is observed, with responsivity as high as 1.82 A W^{-1} (biased at −20 V) under 405 nm LED illumination.

Table 2. Comparison of the results of three In_2O_3 samples and ITO.

Parameters	Sample A	Sample B	Sample C	ITO
Barrier height (eV)	0.95	0.86	0.76	0
Dark current at −20 V bias (nA)	−1.8	−40	−9000	-1.286×10^8
Photogenerated current to dark current ratio, at−20 V bias	470 nm 405 nm 340 nm 280 nm	3.2 36.3 82 120	6 15 12 12	No response

For sample B, at −20 V bias, the dark current increases to 40 nA compared to 1.8 nA of sample A, although the photogenerated currents are still hundreds of nanoamperes. The photogenerated current to dark current ratios of sample B are significantly reduced.

For sample C, nonlinear *I–V* curves are still observed as shown in figure 5(*c*), although the rectification behavior becomes less significant. In this case, the dominant current conduction mechanism over the barrier by thermal emission is accompanied by tunneling through the barrier. This effectively reduces the barrier height as shown in the following analysis. In addition, there are no significant photogenerated currents and the dark current of sample C increases to 9 μA at −20 V bias.

For commercial ITO-coated quartz with sheet resistance about 30 Ω cm^{-2}, the linear *I–V* plot indicates that a good resistance element is shown in figure 5(*d*) and the barrier height here is zero. The tunneling model is dominating in this sample

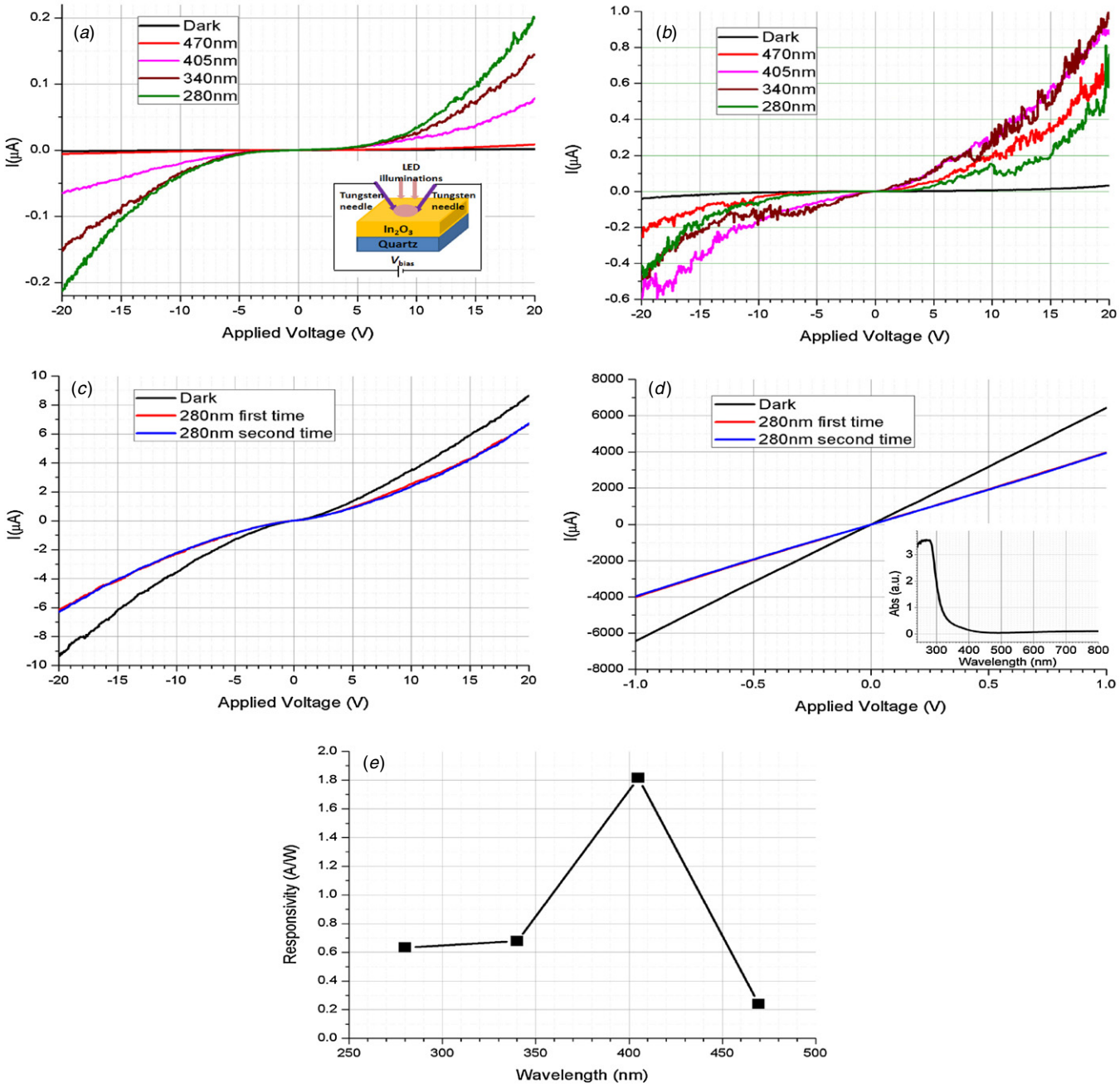

Figure 5. *I–V* plot of (*a*) sample A (In_2O_3), (*b*) sample B (In_2O_3: PVA = 100:1), (*c*) sample C (In_2O_3: PVA = 10:1) and (*d*) ITO with absorption curve in the inset, and (*e*) the rough spectral responsivity of sample A. The inset in (*a*) is the schematic structure for the *I–V* measurement.

instead of the thermal emission model. The dark current of ITO increases to 6.43 mA when the bias is −1 V. Also no significant photoresponse is observed.

In the order of samples A, B, C and ITO, the dark current increases notably, the samples become more resistive and the photoresponse becomes less significant until it disappears. The Schottky barrier formation mechanism in these samples is under investigation. A schematic diagram of the change of barrier height among these samples is shown in figure 6. It appears that imperfections at the semiconductor surface as well as the capping layer such as PVA play an important role during contact formation. Here, the imperfection of In_2O_3 nanorods helps to form the Schottky contacts and creates a MSM photodetector with significant photoresponse. When the barrier heights are lowered like in sample C or commercial ITO, the dark currents become large and dominate the total current even when they are under illumination of LEDs, so the small photogenerated currents are not noticeable compared to large dark currents. Besides that, the high surface area to volume ratio of nanorods increases the absorption of light over traditional bulk or epitaxial grown materials. Hence, the

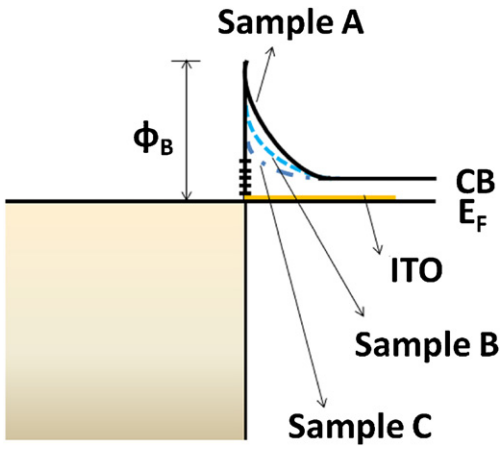

Figure 6. Schematic diagram of the Schottky barrier height of samples A (In_2O_3), B (In_2O_3: PVA = 100:1), C (In_2O_3: PVA = 10:1) and ITO.

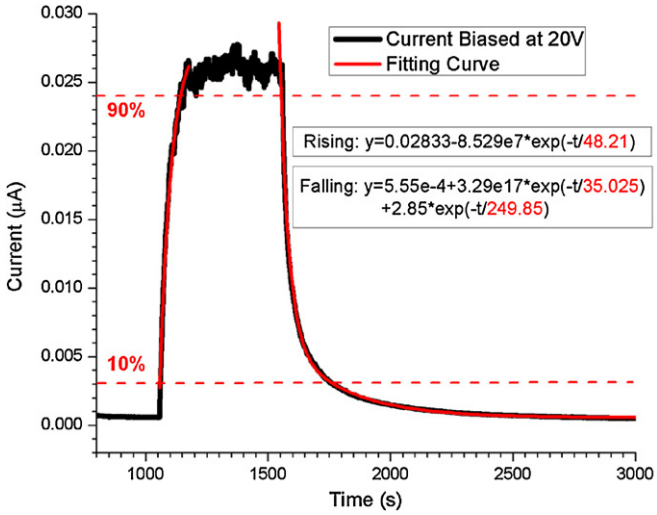

Figure 7. Time-resolved photocurrent of In_2O_3 nanorods.

detector sensitivity can be enhanced by using nanorods as opposed to thin films or bulk materials.

As indicated in figure 7, at 20 V bias, the time response of sample A is close to the reported value [14–16] of more than 35 s. The rising time follows exponential law with a time constant of 48 s. The falling time consists of two exponentials including a fast and slow component with time constants of 35 and 250 s, respectively. The long time response precludes it from high-speed applications. This is a common problem of nanomaterial photodetectors [14–21]. In these devices, the oxygen is absorbed and catches the free electron to form ionized oxygen on the surface of nanomaterials. When light within the band gap of material illuminates the thin film formed by nanomaterials, part of photogenerated holes neutralize the ionized oxygen and release oxygen, while the other photogenerated carriers are collected by the terminals under the electrical field created by the applied voltage. The absorption and release process of oxygen in the surface of nanomaterials is very slow, which dominates the time response of these detectors. But the high ratio of photocurrent to dark current is very attractive for high-sensitivity optical sensors. In addition, completely depleted vertical Schottky device structures have been studied to increase the time response while maintaining the good photoconductive performance of nanoparticle photodetectors [22].

4. Summary

In conclusion, the photoresponse of In_2O_3 nanorods has been studied. The results show that the surface of nanorods plays an important role in the formation of Schottky contact and the absorption of light, which contributes to the significant photoresponse of nanorods compared to thin film and bulk materials. The rough responsivity of In_2O_3 nanorods in the wavelength range of 280–470 nm has been observed. Although the time response needs to be significantly improved for use in high-speed applications, the wavelength-dependent photocurrent as well as the high ratio of photocurrent to dark current is very attractive for the design of high-sensitivity optical sensors.

Acknowledgments

The authors gratefully acknowledge support from National Security Technologies through NSF Industry/University Cooperative Research Center Connection One. The authors also acknowledge the National Science Foundation Smart Lighting Engineering Research Center (EEC-0812056).

References

[1] Walsh A *et al* 2008 Nature of the band gap of In_2O_3 revealed by first-principles calculations and x-ray spectroscopy *Phys. Rev. Lett.* **100** 167402
[2] King P D C *et al* 2009 Band gap, electronic structure, and surface electron accumulation of cubic and rhombohedral In_2O_3 *Phys. Rev.* B **79** 205211
[3] Korobov V, Leibovitch M and Shapira Y 1993 Indium oxide Schottky junctions with InP and GaAs *J. Appl. Phys.* **74** 3251–6
[4] Zheng M J, Zhang L D, Li G H, Zhang X Y and Wang X F 2001 Ordered indium-oxide nanowire arrays and their photoluminescence properties *Appl. Phys. Lett.* **79** 839–41
[5] Zheng M, Zhang L, Zhang X, Zhang J and Li G 2001 Fabricaton and optical absorption of ordered indium oxide nanowire arrays embedded in anodic alumina membranes *Chem. Phys. Lett.* **334** 298–302
[6] Zhou H, Cai W and Zhang L 1999 Photoluminescence of indium-oxide nanoparticles dispersed within pores of mesoporous silica *Appl. Phys. Lett.* **75** 495–7
[7] Fung M K, Sun Y C, Ng A M C, Djurisic A B and Chan W K 2011 Indium tin oxide nanowires growth by dc sputtering *Curr. Appl. Phys.* **11** 594–7
[8] Kuo C, Lu S and Wei T 2005 In_2O_3 nanorod formation induced by substrate structure *J. Cryst. Growth* **285** 400–7
[9] Sun Q, Zeng Y, Zuo K and Jiang D 2011 Alkali tuning phases and morphologies of Ni^{2+} doped In_2O_3 nanocrystals *J. Cryst. Growth* **324** 1–6
[10] Yan Y, Zhang Y, Zeng H, Zhang J, Cao X and Zhang L 2007 Tunable synthesis of In_2O_3 nanowires, nanoarrows and nanorods *Nanotechnology* **18** 175601
[11] Ding G Q, Shen W Z, Zheng M J and Zhou Z B 2006 Indium oxide 'rods in dots' nanostructures *Appl. Phys. Lett.* **89** 063113

[12] Huang Y, Yu K, Xu Z and Zhu Z 2011 Novel In_2O_3 nanostructures fabricated by controlling the kinetics factor for field emission display *Physica* E **43** 1502–8
[13] Shur M 1996 *Introduction to Electronic Devices* (New York: Wiley) p 245
[14] Zhang D, Li C, Han S, Liu X, Tang T, Jin W and Zhou C 2003 Ultraviolet photodetection properties of indium oxide nanowires *Appl. Phys.* A **77** 163–6
[15] Brinzaria V, Ivanova M, Chob B K, Kameic M and Korotcenkov G 2010 Photoconductivity in In_2O_3 nanoscale thin films: interrelation with chemisorbed-type conductometric response towards oxygen *Sensors Actuators* B **148** 427–38
[16] Kim S S, Park J Y, Choi S, Kim H S, Na H G, Yang J C and Kim H W 2010 Significant enhancement of the sensing characteristics of In_2O_3 nanowires by functionalization with Pt nanoparticles *Nanotechnology* **21** 415502
[17] Bi Z, Zhang J, Bian X, Wang D, Zhang X, Zhang W and Hou Z 2008 A high-performance ultraviolet photoconductive detector based on a ZnO film grown by RF sputtering *J. Electron. Mater.* **37** 760–3
[18] Soci C, Zhang A, Xiang B, Dayeh S A, Aplin D P R, Park J, Bao X Y, Lo Y H and Wang D 2007 ZnO nanowire UV photodetectors with high internal gain *Nano Lett.* **7** 1003–9
[19] Li H, Wu G, Shi M, Yang L, Chen H and Wang M 2008 ZnO/ poly(9,9-dihexylfluorene) based inorganic/ organic hybrid ultraviolet photodetector *Appl. Phys. Lett.* **93** 153309
[20] Seong H, Yun J, Jun J H, Cho K and Kim S 2009 The transfer of charge carriers photogenerated in ZnO nanoparticles into a single ZnO nanowire *Nanotechnology* **20** 245201
[21] Qin L, Shing C and Sawyer S 2011 Metal-semiconductor-metal ultraviolet photodetectors based on zinc-oxide colloidal nanoparticles *IEEE Electron Device Lett.* **32** 51–3
[22] Clifford J P, Konstantatos G, Johnston K W, Hoogland S, Levina L and Sargent E H 2009 Fast, sensitive and spectrally tuneable colloidal-quantum-dot photodetectors *Nature Nanotechnol.* **4** 40–4